

A Benchmark for Vision-Centric HD Mapping by V2I Systems

Miao Fan^{1,*}, Shanshan Yu², Shengtong Xu³, Kun Jiang⁴, Haoyi Xiong⁵, and Xiangzeng Liu⁶

Abstract—Autonomous driving faces safety challenges due to a lack of global perspective and the semantic information of vectorized high-definition (HD) maps. Information from roadside cameras can greatly expand the map perception range through vehicle-to-infrastructure (V2I) communications. However, there is still no dataset from the real world available for the study on map vectorization onboard under the scenario of vehicle-infrastructure cooperation. To prosper the research on online HD mapping for Vehicle-Infrastructure Cooperative Autonomous Driving (VICAD), we release a real-world dataset, which contains collaborative camera frames from both vehicles and roadside infrastructures, and provides human annotations of HD map elements. We also present an end-to-end neural framework (i.e., V2I-HD) leveraging vision-centric V2I systems to construct vectorized maps. To reduce computation costs and further deploy V2I-HD on autonomous vehicles, we introduce a directionally decoupled self-attention mechanism to V2I-HD. Extensive experiments show that V2I-HD has superior performance in real-time inference speed, as tested by our real-world dataset. Abundant qualitative results also demonstrate stable and robust map construction quality with low cost in complex and various driving scenes. As a benchmark, both source codes and the dataset have been released at OneDrive¹ for the purpose of further study.

Index Terms—Vehicle-to-Infrastructure (V2I), HD maps, vision-centric, benchmark.

I. INTRODUCTION

High-definition (HD) maps [1] are the most fundamental component of autonomous driving systems, providing centimeter-level details of traffic elements, vectorized topology, and navigation information. HD maps instruct the ego-vehicle to precisely locate itself on the road and anticipate what is coming up ahead. Currently, traditional SLAM-based solutions [2], [3], [4] have been widely adopted in practice. However, challenges such as high annotation costs and delayed updates have led to a gradual shift from offline approaches to learning-based online HD map construction using onboard sensors. Recently, online HD maps constructed in real-time around the ego vehicle using onboard sensors have effectively addressed these issues.

Recent works employ vehicle-mounted surround view perception and point cloud data to enable end-to-end construction of high-definition (HD) maps. Despite advances in single-vehicle perception, they are restricted to limited field

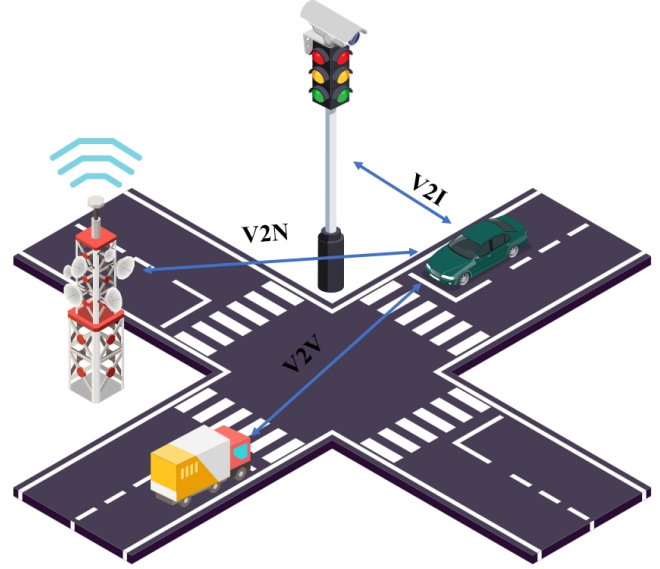


Fig. 1. Cooperative systems in autonomous driving. A comprehensive autonomous driving perception system is composed of the ego vehicle and cooperative interactions among vehicles, infrastructure, and networks.

of view, occlusions, and short-range perception, which result in suboptimal performance in these scenarios. Additionally, compared to offline maps, online HD map construction also encounters inherent limitations stemming from on-vehicle sensors and real-time road conditions. These challenges include variations in data quality caused by swift movement and limitations in the sensor field of view.

A promising solution to address these challenges is to leverage infrastructure information through Vehicle-to-Everything (V2X) communication, which has been proven to significantly extend perception range and improve the safety of autonomous driving, as shown in Fig. 1. Intelligent roadside infrastructure or roadside units (RSUs) equipped with sensors provide uninterrupted and continuous observations with an extensive field of view. These observations enable real-time updates to the dynamically evolving HD map, enhancing its overall perceptual accuracy. Recently, several datasets have been collected from a roadside perspective, making them particularly valuable for advancing perception algorithms in V2X systems. However, these datasets are deficient in certain map element annotations, limiting their applicability for HD map construction.

According to the work mentioned, it can be recognized that unified map element annotations of camera images from the roadside perspective encompassing diverse traffic

¹Chief scientist at NavInfo Co. Ltd., China. Senior member of IEEE.

²Engineer at NavInfo Co. Ltd., China.

³Principal product manager at Autotome Inc., China.

⁴Associate professor at Tsinghua University, China.

⁵Principal scientist at Baidu Inc., China. Senior member of IEEE.

⁶Associate professor at Xidian University, China.

*Correspondence: miao.fan@ieee.org.

¹<https://1drv.ms/f/c/76645c25a8914a0b/EgWY5XCUK6pKqVtE9vB-HbVEBCdCqJvJvgx1KKjeKF7hPdZw>

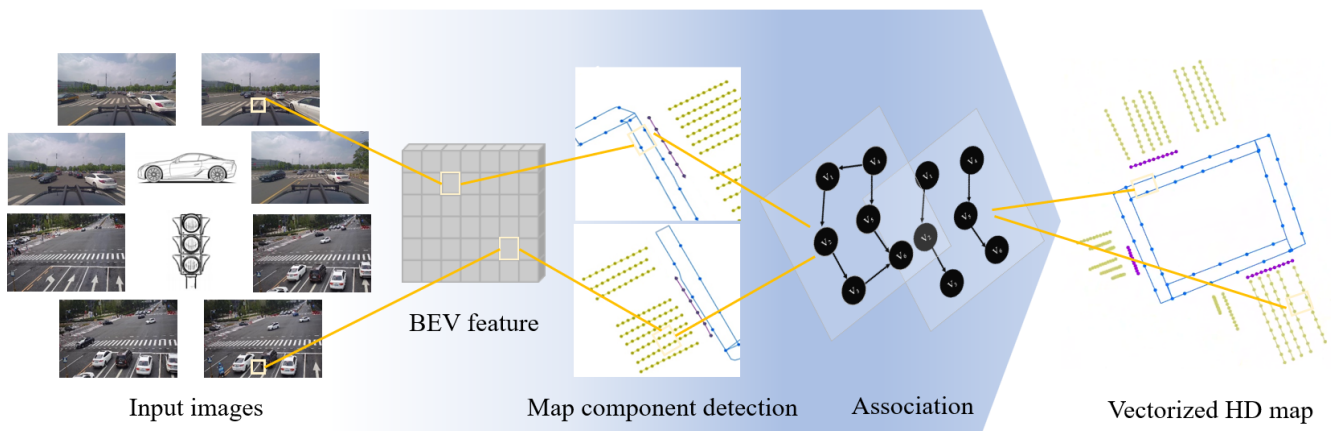


Fig. 2. The pipeline of V2I-HD framework. V2I-HD is a hybrid architecture that combines CNNs with DETR, for real-time HD map learning in a BEV representation. Starting with the input of collaborative camera frames from vehicles and infrastructures, a unified BEV representation is extracted by projecting and fusing image features. The V2I-HD models the map elements through an equivalent vectorized point set, with the final vectorized HD map elements generated throughout the DETR architecture.

participants and scenarios remain rare. The DAIR-V2X-Seq dataset [5] encompassing 2D/3D object annotations sampled from the real world, designed for trajectory tracking and prediction in vehicle-infrastructure collaboration. However, with the lack of vectorized annotations for HD map elements, we release a dataset inherited from DAIR-V2X-Seq, which encompasses corresponding HD map element annotations by cropping vector maps from frames captured by vehicle-mounted and roadside cameras, making it appropriate for HD map construction tasks in V2I contexts. To our knowledge, the transformed dataset is the first release that focuses on HD map construction, making it an ideal resource for the development and evaluation of cooperative perception.

We further propose a novel method called V2I-HD, which copes with creating HD maps onboard for autonomous driving at a minimal cost while achieving superior state-of-the-art performance. In our design, infrastructure cameras from a bird’s eye view cooperate with the front-view image of a vehicle [6] to construct HD maps. V2I-HD initially extracts features from both vehicle&infrastructure-side images, and subsequently transforms these features into a cohesive BEV representation via a map encoder. Then, we leverage the map decoder to estimate and update the map topology. The map decoder comprises map queries and decoder layers. Each decoder layer updates the map query utilizing a direction-decoupled attention scheme.

The contributions of this paper are thus the following:

- We release a real-world dataset, which contains collaborative camera frames from both vehicles and roadside infrastructures and provides HD map element annotations.
- We propose a structured end-to-end framework for efficient online vectorized HD map construction, building on DETR. To reduce computation costs, we introduce directionally decoupled self-attention.
- We demonstrate the capabilities of the solution on

the map and traffic data, and conduct a quantitative assessment of the algorithm to a sub-optimal methods.

This work is structured as follows: Section II discusses related work. Section III presents the problem formulation, neural architecture, and our training strategy. Implementation and experiments are described in sections IV. Finally, section V gives a conclusion.

II. RELATED WORK

This section reviews related work concerning HD map construction under Vehicle-to-Infrastructure (V2I) communication, deriving information from available datasets.

A. Vectorized HD Map Construction

HD maps consist of geometric objects and semantic properties, both of which are crucial for downstream tasks. HD map construction in BEV space [7], [8] relies on data gathered by onboard sensor observations, encompassing RGB images from multi-view cameras and point clouds from LiDAR. Current methodologies for HD map construction can be broadly classified into two categories: rasterized HD map estimation [9], [10], [11], [12] and vectorized HD map construction [7], [13], [14], [15]. Rasterized HD maps often require extensive post-processing, making them less ideal for downstream tasks. In contrast, vectorized HD map construction addresses these constraints by representing maps using a collection of map elements. For instance, VectorMapNet [14] explores the keypoint-based representation within a hierarchical two-stage network. InsightMapper [16] demonstrates the benefits of leveraging internal instance point data. The MapTR series [13], [17] introduces permutation-equivalent modeling of point sets and a DETR-like [18] single-stage network. Recent works have focused on learning element-level information. For example, MapVR [19] incorporates differentiable rasterization and enhances supervision through element-level segmentation. BeMapNet [15] initially identifies map elements and subsequently enhances detailed nodes

with a segmented Bezier head. PivotNet [7] proposes a Point-to-Line Mask module, which transforms point-level representations into element-level representations.

However, all of the above work relies on HD map constructed by sensors from the vehicle ego, whose perception has long suffered from limitations of range restrictions, sensor field of view, and occlusions. The National Highway Transportation and Safety Authority (NHTSA) has outlined several scenarios in which occlusions may result in traffic collisions [20]. In one such scenario (Fig. 3), the black vehicle, equipped with a front view camera, will collide with an oncoming yellow vehicle that is disregarding a red light, as a red truck obstructs its frontal view. If the black vehicle had seen the oncoming vehicle, it might have averted the collision. A potential solution to this problem is the implementation of intelligent roadside infrastructure or Roadside Units (RSUs) to enhance the vehicle’s sensor range. Early work from He [21] utilized roadside infrastructure to enhance the vehicle’s field of vision, facilitating real-time map inference. Compared with other state-of-the-art methods of online HD inferencing, this solution significantly improved the safety of autonomous driving. In this study, we propose a structured end-to-end framework for the development of HD maps to enhance both accuracy and coverage. Different from He’s method, our method employs only roadside cameras and the vehicle’s front-facing camera.

B. Available Datasets

Table I presents a summary of the datasets utilized for the construction of HD maps. Four original datasets, specifically Argoverse 1 and 2 [22], [23], nuScenes [24], Waymo [25], and DAIR-V2X-Seq [5], provide the HD map data necessary for online map inference. These datasets with comprehensive object annotations are mainly designed for object tracking and trajectory prediction tasks, encompassing vehicle-point clouds and images. Although these publicly available datasets facilitate fair and consistent evaluation in research, they were initially designed for dynamic object perception rather than HD map inference. To avert sample overlap within a sequence, the datasets are temporally divided but do not ensure geographic separation. Despite this, nuScenes [24] and Argoverse 2 [23] are widely used for training online mapping models and have become the de facto standard.

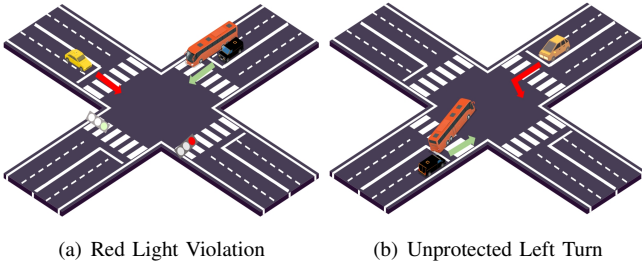


Fig. 3. The red truck(s) block the black vehicle’s view. It cannot see the oncoming yellow vehicle violating the red light in (a) and taking the unprotected left turn in (b).

Nevertheless, numerous research have employed nuScenes or Argoverse 2 to train online mapping models, which have emerged as de facto standards in the domain. For example, online mapping methods using nuScenes include [26], [27], [10], [9] and Argoverse 2 is used in [13], [17]. Both nuScenes and Argoverse 2 are devoid of data from roadside sensors, hence constraining their use in V2I scenarios. DAIR-V2X-Seq encompasses infrastructure-based data; nevertheless, this dataset is tailored for object tracking and trajectory prediction tasks, rendering it unapplicable for map inference. This work releases a dataset specifically created for the online inference of HD maps, featuring annotations of map components related to both vehicle-side and roadside images.

III. METHODS

Here, we describe how we model the problem, construct our network, and further minimize computational cost.

A. Problem Formulation

By sampling the sequence of components in the vector map, each feature can be represented as curves of varying shapes. Following the methodology presented in MapTRv2 [17], we encapsulate map features into closed geometries (e.g., crosswalks) and open geometries (e.g., divider lines, stop lines). Uniform sequential sampling along feature boundaries abstracts the geometric representation of closed shapes as polygons and open shapes as polylines.

Each map element corresponds to $\mathcal{V} = (V, \Gamma)$. $V = \{v_j\}_{j=0}^{N_v-1}$ denotes a collection of points of the map element (N_v is the number of points). $\Gamma = \gamma^k$ signifies a group of equivalent permutations of the point set V , including all potential permutations of the specified map feature. Specifically, for polyline element with unspecific direction, Γ includes 2 kinds of equivalent permutations:

$$\begin{aligned} \Gamma_{\text{polyline}} &= \{\gamma^0, \gamma^1\} \\ &= \begin{cases} \gamma^0(j) = j\%N_v \\ \gamma^1(j) = (N_v - 1) - j\%N_v \end{cases} \end{aligned} \quad (1)$$

For a polyline element with a specified direction, Γ includes only one permutation: γ^0 .

For polygon element, Γ includes $2N_v$ kinds of equivalent permutations:

$$\begin{aligned} \Gamma_{\text{polygon}} &= \{\gamma^0, \dots, \gamma^{2 \times N_v - 1}\} \\ &= \begin{cases} \gamma^0(j) = j\%N_v \\ \gamma^1(j) = (N_v - 1) - j\%N_v \\ \gamma^2(j) = (j + 1)\%N_v \\ \gamma^3(j) = (N_v - 1) - (j + 1)\%N_v \\ \dots \\ \gamma^{2 \times N_v - 2}(j) = (j + N_v - 1)\%N_v \\ \gamma^{2 \times N_v - 1}(j) = (N_v - 1) - (j + N_v - 1)\%N_v \end{cases} \end{aligned} \quad (2)$$

B. Neural Architecture

The comprehensive model architecture is depicted in detail in Fig. 2, which delineates the framework into three components: feature extractor, Map Encoder, and Map Decoder.

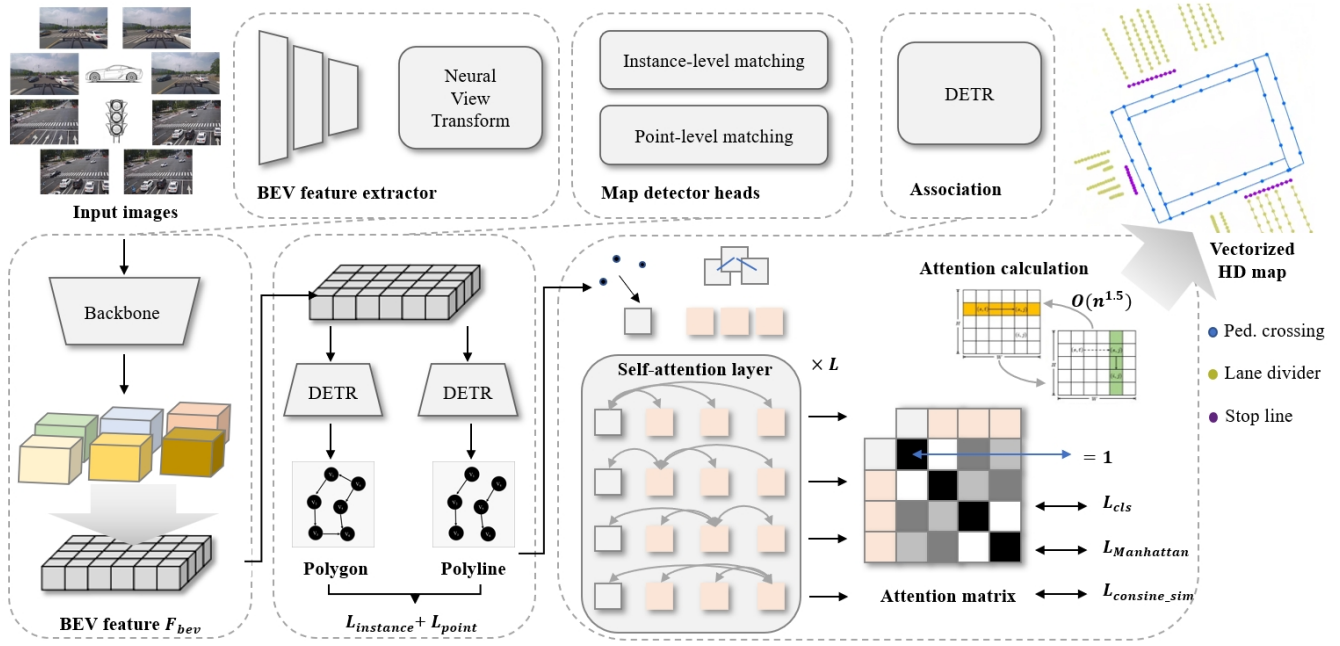


Fig. 4. The framework of V2I-HD . The upper blocks show the main components of V2I-HD, and the lower blocks provide detailed information regarding the structure and training of each component.

TABLE I
DATASETS USED FOR ONLINE MAPPING.

Dataset	Split	Source	Main Map Purpose	#Samples			Geo.Split
				Train	Valid	Test	
nuScenes	Original	nuSc	OD/MF	28K	6K	6K	✗
Argoverse 1	Original	argo1	OD/MF	39K	15K	13K	✓
Argoverse 2	Original	argo2	OD/MF	110K	24K	24K	✗
Waymo	Original	way	OD/MF	122K	30K	40K	✗
nuScenes	Near	nuSc	OM	28K	6K	6K	✓
Argoverse 2	Near	argo2	OM	110K	24K	24K	✓
nuScenes	Far-A	nuSc	OM	30K	9K	-	✓
nuScenes	Far-B	nuSc	OM	31K	9K	-	✓
Argoverse 2	Far-A	argo2	OM	110K	46K	-	✓
Argoverse 2	Far-B	argo2	OM	101K	55K	-	✓
Argoverse 2	Far-C	argo2	OM	101K	55K	-	✓

Datasets used for HD map construction. The proposed splits are shown in bold. OD = object detection, MF = motion forecasting, OM = online mapping.

1) *Feature extractor*: With inputs of images from the vehicle’s front-facing camera and the overhead roadside view, we initially extract features from each image employing a common CNN backbone. Then, multi-scale features from various phases are fed into a Feature Pyramid Network (FPN) [28] to integrate comprehensive semantic information. Ultimately, we upsample the pyramid features to a uniform size and stack them as the final output.

2) *Map encoder*: We utilize a conventional Transformer-based architecture to consistently convert image attributes into the BEV space. The BEV decoder models the task as a set prediction problem using perspective transformation,

which takes camera features with shape $H_c \times W_c$ and $H_q \times W_q$ queries as inputs and produces BEV features $F_b \in \mathbb{R}^{C \times H_b \times W_b}$ by modeling all pairwise interactions among elements with self-attention. Currently, other PV2BEV approaches exist, e.g., CVT [29], LSS [30], Deformable Attention [10], GKT [31] and IPM [32]; however, given that our model must be implemented on the vehicle side, we have chosen GKT as the default transformation method.

3) *Map decoder*: The map decoder comprises map queries and many decoder layers, with each layer enhancing the element queries via attention mechanisms. Current methodologies modify queries utilizing raw attention, leading

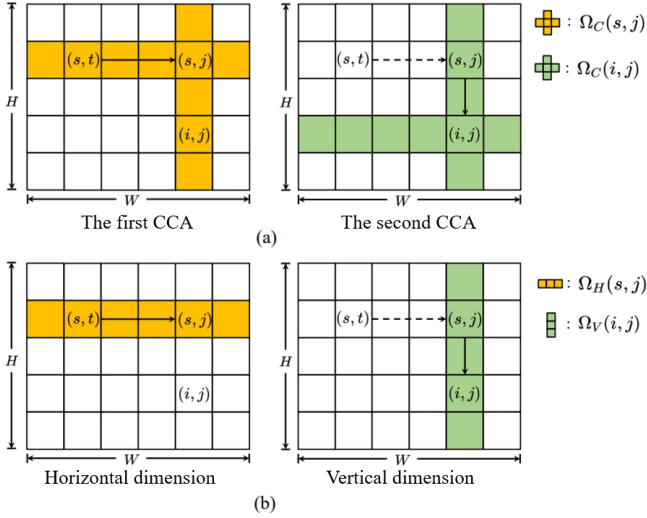


Fig. 5. The difference between the attention component of RCCA and a non-local similarity algorithm using direction decoupling.

to a computational complexity of $O((N \times N_v)^2)$, where N and N_v denote the quantities of instance queries and point queries, respectively. As the volume of requests escalates, the computing expense rises rapidly. To alleviate this computational burden, we employ direction-decoupled self-attention, which initially calculates attention in the horizontal direction followed by the vertical direction. This method enables the vertical attention computation to integrate information from the horizontal direction, as depicted in Figure 5. Decoupled self-attention decreases the computational complexity from $O((N \times N_v)^2)$ to $O((N \times N_v)^{1.5})$ [33] and outperforms the conventional self-attention technique.

4) *Output head*: Utilizing the methodology described in the problem modeling section, we construct a segmented output head that incorporates both instance matching and point-level matching. Initially, the instance class scores are forecasted, succeeded by the regression of point-level distance losses. The outputs are produced by amalgamating these predictions, resulting in a vector of dimension $2N_v$ or $2N_v$, which signifies normalized 2D or 3D coordinates of the N_v points.

C. End-to-End Training

1) *Ground truth*: The DAIR-V2X-Seq dataset is deficient in camera depth parameters, rendering direct projection of the pictures into the world coordinate system unfeasible. To address this problem, we correlate the point cloud data with the image data to generate depth maps, which are subsequently employed to align the images with the HD map in the world coordinate system, facilitating the annotation of map features. The map feature annotations are efficiently represented as curves utilizing a collection of vector points. These annotations data are released via our dataset.

2) *Loss function*: The framework is trained via instance matching and point set regression. The fundamental loss function comprises three components: classification loss,

point-to-point loss, and edge direction loss:

$$\begin{aligned} \mathcal{L}_{\text{one2one}} &= \mathcal{L}_{\text{Hungarian}}(\hat{Y}, Y) \\ &= \lambda_c \mathcal{L}_{\text{cls}} + \lambda_p \mathcal{L}_{\text{p2p}} + \lambda_d \mathcal{L}_{\text{dir}} \end{aligned} \quad (3)$$

Each predicted map element is designated a class label based on the instance-level optimal matching outcome. The classification loss is defined as a Focal Loss term formulated as:

$$\mathcal{L}_{\text{cls}} = \sum_{i=0}^{N-1} \mathcal{L}_{\text{Focal}}(\hat{p}_{\hat{\pi}(i)}, c_i). \quad (4)$$

Point-to-point loss regulates the position of each predicted point. For each ground truth (GT) instance indexed by i , based on the point-level optimal matching result $\hat{\gamma}_i$, each predicted point $\hat{v}_{\hat{\pi}(i),j}$ is allocated to a GT point $v_{i,\hat{\gamma}_i(j)}$. The point-to-point loss is defined as the Manhattan distance calculated between each assigned point pair:

$$\mathcal{L}_{\text{p2p}} = \sum_{i=0}^{N-1} \mathbb{1}_{\{c_i \neq \emptyset\}} \sum_{j=0}^{N_v-1} D_{\text{Manhattan}}(\hat{v}_{\hat{\pi}(i),j}, v_{i,\hat{\gamma}_i(j)}). \quad (5)$$

Point-to-point loss exclusively supervises the vertex of the polyline and polygon, disregarding the edge. The orientation of the edge is crucial for the precise representation of map elements. Consequently, we furthermore formulate edge direction loss to regulate the geometric configuration at the elevated edge level:

$$\mathcal{L}_{\text{dir}} = - \sum_{i=0}^{N-1} \mathbb{1}_{\{c_i \neq \emptyset\}} \sum_{j=0}^{N_v-1} \cos_similarity(\hat{e}_{\hat{\pi}(i),j}, e_{i,\hat{\gamma}_i(j)}), \quad (6)$$

IV. EXPERIMENTS

A. Experimental Settings

1) *Dataset*: To evaluate the proposed approach, our dataset comprises 10669/4585 samples for the training/validation set from 28 intersections. Each scene consists of around 545 samples, with each sample including 8 images, including 4 frames from the vehicle's front-facing camera and 4 frames from the roadside overhead camera. To provide an equitable assessment, we concentrate on three static map classifications, as delineated in other studies: lane dividers, stop lines and pedestrian crossings. The perceptual range centered on the ego vehicle is established at [30, 30, 15, 15] meters, representing the distances to the front, rear, left, and right, respectively. Furthermore, we establish the resolution of the ego-to-pixel transformation at 0.15 m/pixel.

2) *Evaluation metrics*: We evaluate the quality of map production by Average Precision (AP). Average Precision (AP) is determined by assessing the chamfer distance between a ground truth and a forecasted value, with a prediction deemed a true positive only if its distance falls below a specified threshold. In our trials, this threshold is established at [0.2, 0.5, 1.0] meters. The mean Average Precision (AP) is calculated by averaging the AP across the three mapping categories.

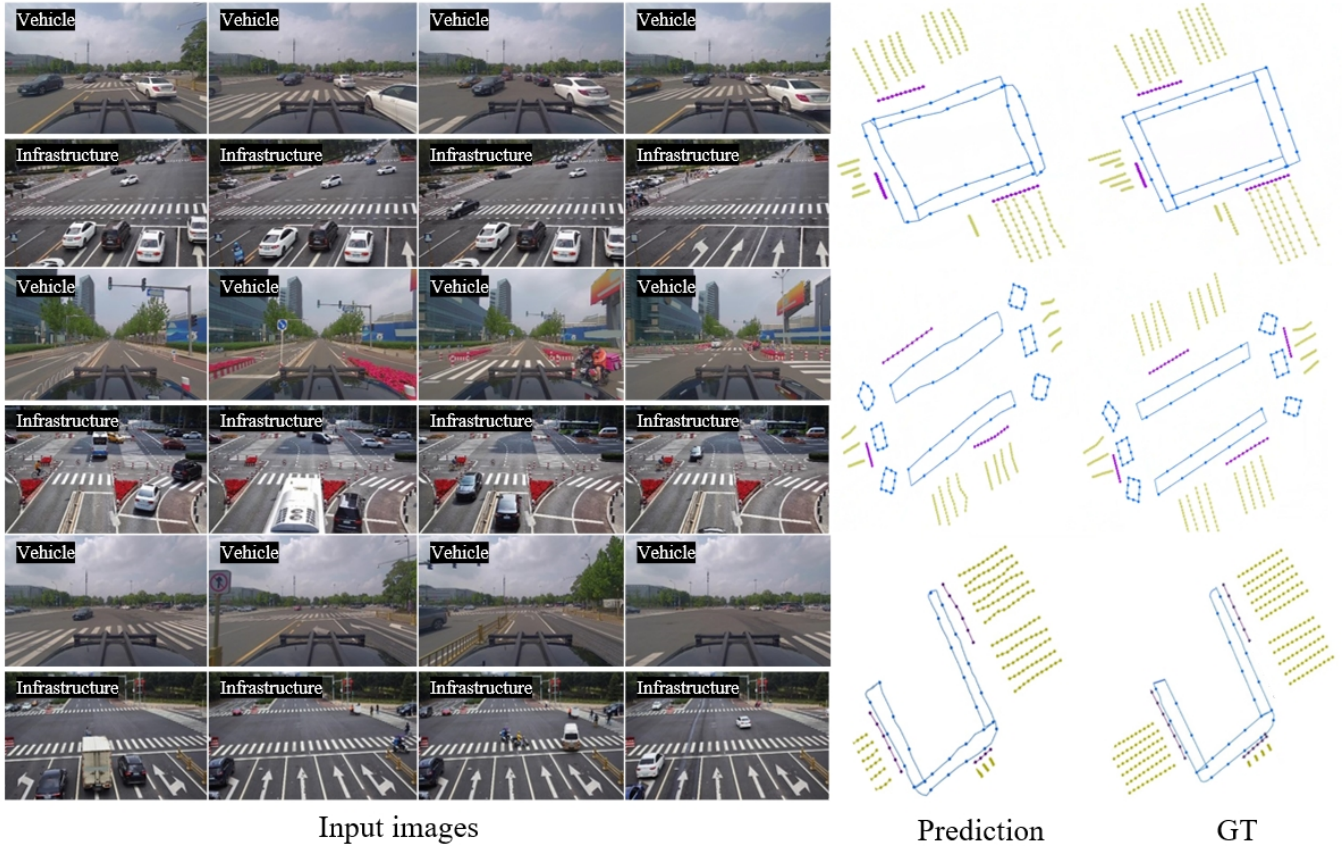


Fig. 6. Qualitative results of V2I-HD on complex traffic scenes under various conditions. Lane dividers, stoplines, and pedestrian crossings are visualized in yellow, blue, and purple.

TABLE II
EVALUATION RESULTS ON V2X SEQ DATASET.

Method	Modality	Backbone	Epochs	AP			mAP	FPS
				pedestrian crossing	lane divider	stop line		
HDMaNet [9]	V	EffiNet-B0	30	12.0	5.2	18.9	12.0	-
HDMaNet [9]	V&I	EffiNet-B0	30	14.8	8.1	23.3	15.5	-
MapTR [13]	V	R18	110	21.6	23.5	23.8	22.9	38.2
MapTR [13]	V&I	R18	110	32.8	38.4	39.5	36.9	10.5
MapTR [13]	V	R50	110	26.8	32.1	34.6	31.1	16.5
MapTR [13]	V&I	R50	110	36.7	42.2	43.5	40.8	6.4
V2I-HD	V	R18	110	24.5	26.0	27.2	25.9	44.5
V2I-HD	V&I	R18	110	36.8	39.6	40.2	38.9	18.8
V2I-HD	V	R50	110	28.4	30.5	32.8	30.5	20.8
V2I-HD	V&I	R50	110	41.4	45.5	47.8	44.9	9.6

Performance comparison with baseline methods at V2I sense on V2X Seq provided by the HD map construction challenge. 'V' denotes input data originating solely from the vehicle, while 'V&I' refers to input data that includes contributions from both the vehicle and the infrastructure. The quantitative findings demonstrate that our V2I-HD substantially enhances HD map production and surpasses baseline methods.

3) *Implementation details:* We utilize ResNet-50/ResNet-18 and DETR as backbones, both initialized using ImageNet pretraining. The semantic BEV decoder comprises two transformer encoder layers, with default quantities of 50 for queries, 20 for point queries, and 6 for decoder layers. The input image dimensions are adjusted to 1920×1080 , with a mini-batch size of 1 per RTX 3090 GPU. We train our model

using 1 RTX 3090 GPU for 30/110 epochs and implement a multi-step schedule with milestones at $[0.7, 0.9]$ and $\gamma = \frac{1}{3}$. The Adam optimizer utilizes a weight decay of 1×10^{-4} and a learning rate of 2×10^{-4} , which is subsequently multiplied by 0.1 for the backbone. We assigned the hyper-parameters for loss weight as follows: $\lambda_s = 1$, $\lambda_z = 5$, $\lambda_p = 5$, $\lambda_c = 10$, and $\lambda_r = 1$. Additionally, the dilated width ω in $\mathcal{L}_{\text{region}}$ was

TABLE III
ABLATION ON ATTENTION CALCULATION.

Self-Attn	Backbone	AP			mAP	GPU memory	FPS
		pedestrian crossing	lane divider	stop line			
Vanilla	R18	26.1	28.4	30.0	28.1	11621 MB	15.3
Vanilla	R50	28.8	30.9	32.3	30.6	13952 MB	15.3
RCCA	R18	32.7	34.5	36.0	34.4	9753 MB	15.5
RCCA	R50	36.9	39.5	40.5	38.9	12790 MB	15.5
Decoupled	R18	36.8	39.6	40.2	38.9	8930 MB	18.8
Decoupled	R50	40.4	44.5	46.8	43.9	10682 MB	9.6

Ablation of the self-attention variations. The inter self-attention significantly decreases memory consumption while maintaining comparable accuracy. Consequently, we have designated the disconnected self-attention as the standard configuration.

TABLE IV
ABLATION ON BEV EXTRACTOR.

Backbone	Method	mAP	FPS	Param
R18	IPM	17.2	15.4	35.7
	LSS	19.6	12.8	39.2
	GKT	20.8	15.2	36.8
R50	IPM	17.2	15.4	35.7
	LSS	19.6	12.8	39.2
	GKT	20.8	15.2	36.8

Ablation on the BEV extractor. We use the classic models in the BEV feature extractor, such as LSS, and GKT. Considering that the model needs to be deployed on the vehicle side in the future, GKT is used as the conversion module.

set to 5.

B. Comparison Results

As our research is the inaugural exploration of using both automobiles and infrastructure for the creation of high-definition (HD) maps, there are presently no recognized competing methodologies. We additionally adapt existing vehicle-based models to the V2I (vehicle-to-infrastructure) context for vectorized HD map production to facilitate comparison with our approach. Table II presents the use of HDMapNet [9], a leading model for the generation of vectorized HD maps. Our V2I-HD conducts uncertainty-aware fusion on the static BEV (Bird’s Eye View) features derived from the open-source HDMapNet model. The findings indicate that V2I-HD enhances HD map generation quality by more than 5 mAP, illustrating its efficacy in producing superior HD maps within the V2I context. Furthermore, we evaluate V2I-HD in terms of frames per second (FPS), which also utilizes the HD map production inference speed presented in Table II. Our V2I-HD pipeline demonstrates superior performance in both absolute improvement (43.9 mAP compared to 42.8 mAP and 15.5 mAP) and relative improvement (13.9 mAP compared to 11.7 mAP and 3.45 mAP).

We show the vectorized HD map predictions in Fig. 6. It illustrates that V2I-HD has strong generalization across di-

verse situations. V2I-HD calculates, in an end-to-end method without post-processing or intensive computation, the semantic and instance-level data of intricate map elements. Our vector map modeling technique, illustrated in Fig. 4, facilitates precise and rapid prediction of map elements.

C. Ablation Study

This section presents ablation experiments to evaluate the efficacy of the proposed modules and design decisions. All trials are run on our dataset to guarantee a fair comparison, with training spanning 110 epochs. ResNet18 and ResNet50 serve as the picture backbones in the tests.

1) *Ablation on the self-attention variants:* Table III delineates the efficacy of several computational methodologies in the semantic decoder for map generation. The findings utilizing ResNet50 indicate that RCCA [34] markedly decreases training memory use (by 1162M) with just a minimal reduction in accuracy (a decline of 0.2 mAP). Moreover, in comparison to vanilla self-attention [35], decoupled self-attention exhibits greater memory efficiency (decreasing memory use by 2108M), enhances accuracy (increasing by 5 mAP), and preserves comparable speed. Within the same computational parameters, detached self-attention attains inference with markedly less memory usage and accelerated processing speed while maintaining predictive accuracy.

2) *Ablation on BEV extractor:* Table IV presents the approaches for transforming 2D to BEV, encompassing IPM, LSS, and GKT, as well as the application of deformable attention. We employed the optimized implementation of LSS for the trials. To facilitate an even comparison with IPM and LSS, both GKT and deformable attention were configured using decoupled parameters. The findings indicate that V2I-HD is compatible with multiple 2D to BEV methodologies and maintains consistent performance across all configurations.

V. CONCLUSION

In this paper, we release the first dataset for online vectorized HD map construction by vision-centric V2I systems. It contains annotations for both vehicle-side and infrastructure map elements, where all the data elements are captured

from the real world. To provide a benchmark of V2I HD mapping, we present a structured end-to-end framework (i.e., V2I-HD) for efficient vectorized HD map construction onboard leveraging collaborative camera frames from both vehicles and roadside infrastructures. We also introduce a directionally decoupled self-attention mechanism to V2I-HD for the sake of reducing computation costs. Extensive experiments show that V2I-HD has superior performance in map elements of arbitrary shape compared to other methods on our dataset.

ACKNOWLEDGMENTS

This work was sponsored by Beijing Nova Program (No. 20240484616).

REFERENCES

- [1] M. Fan, Y. Yao, J. Zhang, X. Song, and D. Wu, "Neural hd map generation from multiple vectorized tiles locally produced by autonomous vehicles," in *Spatial Data and Intelligence: 5th China Conference, SpatialDI 2024, Nanjing, China, April 25–27, 2024, Proceedings*. Berlin, Heidelberg: Springer-Verlag, 2024, p. 307–318.
- [2] T. Shan and B. Englot, "Lego-loam: Lightweight and ground-optimized lidar odometry and mapping on variable terrain," in *2018 IEEE/RSJ International Conference on Intelligent Robots and Systems (IROS)*. IEEE, 2018, pp. 4758–4765.
- [3] T. Shan, B. Englot, D. Meyers, W. Wang, C. Ratti, and D. Rus, "Lio-sam: Tightly-coupled lidar inertial odometry via smoothing and mapping," in *2020 IEEE/RSJ international conference on intelligent robots and systems (IROS)*. IEEE, 2020, pp. 5135–5142.
- [4] J. Zhang, S. Singh, *et al.*, "Loam: Lidar odometry and mapping in real-time," in *Robotics: Science and systems*, vol. 2, no. 9. Berkeley, CA, 2014, pp. 1–9.
- [5] H. Yu, W. Yang, H. Ruan, Z. Yang, Y. Tang, X. Gao, X. Hao, Y. Shi, Y. Pan, N. Sun, *et al.*, "V2x-seq: A large-scale sequential dataset for vehicle-infrastructure cooperative perception and forecasting," in *Proceedings of the IEEE/CVF Conference on Computer Vision and Pattern Recognition*, 2023, pp. 5486–5495.
- [6] M. Fan, J. Huang, and H. Wang, "Dumapper: Towards automatic verification of large-scale pois with street views at baidu maps," in *Proceedings of the 31st ACM International Conference on Information and Knowledge Management*, ser. CIKM '22. New York, NY, USA: Association for Computing Machinery, 2022, p. 3063–3071.
- [7] W. Ding, L. Qiao, X. Qiu, and C. Zhang, "Pivotnet: Vectorized pivot learning for end-to-end hd map construction," in *Proceedings of the IEEE/CVF International Conference on Computer Vision*, 2023, pp. 3672–3682.
- [8] X. Hao, H. Zhang, Y. Yang, Y. Zhou, S. Jung, S.-I. Park, and B. Yoo, "Mbfusion: A new multi-modal bev feature fusion method for hd map construction," in *2024 IEEE International Conference on Robotics and Automation (ICRA)*. IEEE, 2024, pp. 15 922–15 928.
- [9] Q. Li, Y. Wang, Y. Wang, and H. Zhao, "Hdmapnet: An online hd map construction and evaluation framework," in *2022 International Conference on Robotics and Automation (ICRA)*. IEEE, 2022, pp. 4628–4634.
- [10] Z. Li, W. Wang, H. Li, E. Xie, C. Sima, T. Lu, Y. Qiao, and J. Dai, "Bevformer: Learning bird's-eye-view representation from multi-camera images via spatiotemporal transformers," in *European conference on computer vision*. Springer, 2022, pp. 1–18.
- [11] Z. Liu, H. Tang, A. Amiri, X. Yang, H. Mao, D. L. Rus, and S. Han, "Bevfusion: Multi-task multi-sensor fusion with unified bird's-eye view representation," in *2023 IEEE international conference on robotics and automation (ICRA)*. IEEE, 2023, pp. 2774–2781.
- [12] X. Xiong, Y. Liu, T. Yuan, Y. Wang, Y. Wang, and H. Zhao, "Neural map prior for autonomous driving," in *Proceedings of the IEEE/CVF Conference on Computer Vision and Pattern Recognition*, 2023, pp. 17 535–17 544.
- [13] B. Liao, S. Chen, X. Wang, T. Cheng, Q. Zhang, W. Liu, and C. Huang, "Maptr: Structured modeling and learning for online vectorized hd map construction," *arXiv preprint arXiv:2208.14437*, 2022.
- [14] Y. Liu, T. Yuan, Y. Wang, Y. Wang, and H. Zhao, "Vectormapnet: End-to-end vectorized hd map learning," in *International Conference on Machine Learning*. PMLR, 2023, pp. 22 352–22 369.
- [15] L. Qiao, W. Ding, X. Qiu, and C. Zhang, "End-to-end vectorized hd-map construction with piecewise bezier curve," in *Proceedings of the IEEE/CVF Conference on Computer Vision and Pattern Recognition*, 2023, pp. 13 218–13 228.
- [16] Z. Xu, K. K. Wong, and H. Zhao, "Insightmapper: A closer look at inner-instance information for vectorized high-definition mapping," *arXiv preprint arXiv:2308.08543*, 2023.
- [17] B. Liao, S. Chen, Y. Zhang, B. Jiang, Q. Zhang, W. Liu, C. Huang, and X. Wang, "Maptrv2: An end-to-end framework for online vectorized hd map construction," *arXiv preprint arXiv:2308.05736*, 2023.
- [18] N. Carion, F. Massa, G. Synnaeve, N. Usunier, A. Kirillov, and S. Zagoruyko, "End-to-end object detection with transformers," in *European conference on computer vision*. Springer, 2020, pp. 213–229.
- [19] G. Zhang, J. Lin, S. Wu, Z. Luo, Y. Xue, S. Lu, Z. Wang, *et al.*, "Online map vectorization for autonomous driving: A rasterization perspective," *Advances in Neural Information Processing Systems*, vol. 36, 2024.
- [20] W. G. Najm, R. Ranganathan, G. Srinivasan, J. D. Smith, S. Toma, E. D. Swanson, A. Burgett, *et al.*, "Description of light-vehicle pre-crash scenarios for safety applications based on vehicle-to-vehicle communications," United States. Department of Transportation. National Highway Traffic Safety . . . , Tech. Rep., 2013.
- [21] Y. He, C. Bian, J. Xia, S. Shi, Z. Yan, Q. Song, and G. Xing, "Vi-map: Infrastructure-assisted real-time hd mapping for autonomous driving," in *Proceedings of the 29th Annual International Conference on Mobile Computing and Networking*, 2023, pp. 1–15.
- [22] M.-F. Chang, J. Lambert, P. Sangkloy, J. Singh, S. Bak, A. Hartnett, D. Wang, P. Carr, S. Lucey, D. Ramanan, *et al.*, "Argoverse: 3d tracking and forecasting with rich maps," in *Proceedings of the IEEE/CVF conference on computer vision and pattern recognition*, 2019, pp. 8748–8757.
- [23] B. Wilson, W. Qi, T. Agarwal, J. Lambert, J. Singh, S. Khandelwal, B. Pan, R. Kumar, A. Hartnett, J. K. Pontes, *et al.*, "Argoverse 2: Next generation datasets for self-driving perception and forecasting," *arXiv preprint arXiv:2301.00493*, 2023.
- [24] H. Caesar, V. Bankiti, A. H. Lang, S. Vora, V. E. Liong, Q. Xu, A. Krishnan, Y. Pan, G. Baldan, and O. Beijbom, "nusenes: A multimodal dataset for autonomous driving," in *Proceedings of the IEEE/CVF conference on computer vision and pattern recognition*, 2020, pp. 11 621–11 631.
- [25] P. Sun, H. Kretzschmar, X. Dotiwalla, A. Chouard, V. Patnaik, P. Tsui, J. Guo, Y. Zhou, Y. Chai, B. Caine, *et al.*, "Scalability in perception for autonomous driving: Waymo open dataset," in *Proceedings of the IEEE/CVF conference on computer vision and pattern recognition*, 2020, pp. 2446–2454.
- [26] S. Hu, L. Chen, P. Wu, H. Li, J. Yan, and D. Tao, "St-p3: End-to-end vision-based autonomous driving via spatial-temporal feature learning," in *European Conference on Computer Vision*. Springer, 2022, pp. 533–549.
- [27] Y. Jiang, L. Zhang, Z. Miao, X. Zhu, J. Gao, W. Hu, and Y.-G. Jiang, "Polarformer: Multi-camera 3d object detection with polar transformer," in *Proceedings of the AAAI conference on Artificial Intelligence*, vol. 37, no. 1, 2023, pp. 1042–1050.
- [28] M. Tan, R. Pang, and Q. V. Le, "Efficientdet: Scalable and efficient object detection," in *Proceedings of the IEEE/CVF conference on computer vision and pattern recognition*, 2020, pp. 10 781–10 790.
- [29] B. Zhou and P. Krähenbühl, "Cross-view transformers for real-time map-view semantic segmentation," in *Proceedings of the IEEE/CVF conference on computer vision and pattern recognition*, 2022, pp. 13 760–13 769.
- [30] J. Phillion and S. Fidler, "Lift, splat, shoot: Encoding images from arbitrary camera rigs by implicitly unprojecting to 3d," in *Computer Vision—ECCV 2020: 16th European Conference, Glasgow, UK, August 23–28, 2020, Proceedings, Part XIV 16*. Springer, 2020, pp. 194–210.
- [31] S. Chen, T. Cheng, X. Wang, W. Meng, Q. Zhang, and W. Liu, "Efficient and robust 2d-to-bev representation learning via geometry-guided kernel transformer," *arXiv preprint arXiv:2206.04584*, 2022.
- [32] H. A. Mallot, H. H. Bülthoff, J. J. Little, and S. Bohrer, "Inverse perspective mapping simplifies optical flow computation and obstacle detection," *Biological cybernetics*, vol. 64, no. 3, pp. 177–185, 1991.
- [33] Z. Song, B. Zhong, J. Ji, and K.-K. Ma, "A direction-decoupled non-local attention network for single image super-resolution," *IEEE Signal Processing Letters*, vol. 29, pp. 2218–2222, 2022.

- [34] Z. Huang, X. Wang, L. Huang, C. Huang, Y. Wei, and W. Liu, "Ccnet: Criss-cross attention for semantic segmentation," in *Proceedings of the IEEE/CVF international conference on computer vision*, 2019, pp. 603–612.
- [35] C. Zhou, J. Bai, J. Song, X. Liu, Z. Zhao, X. Chen, and J. Gao, "Atrank: An attention-based user behavior modeling framework for recommendation," in *Proceedings of the AAAI conference on artificial intelligence*, vol. 32, no. 1, 2018.